Electrical and optical characterization of multi-hollow surface dielectric barrier discharge in configuration with the air-exposed electrode

View Online   Export Citation   CrossMark

Richard Cimerman,[1] (iD) Emanuel Maťaš,[2] (iD) Matej Sárený,[3] (iD) and Karol Hensel[1,a] (iD)

AFFILIATIONS

[1]Division of Environmental Physics, Faculty of Mathematics, Physics and Informatics, Comenius University, Mlynská dolina F2, 842 48 Bratislava, Slovakia
[2]Department of Experimental Physics, Faculty of Mathematics, Physics and Informatics, Comenius University, Mlynská dolina F2, 842 48 Bratislava, Slovakia
[3]Department of Theoretical Physics, Faculty of Mathematics, Physics and Informatics, Comenius University, Mlynská dolina F2, 842 48 Bratislava, Slovakia

[a]Author to whom correspondence should be addressed: karol.hensel@fmph.uniba.sk

ABSTRACT

In this paper, multi-hollow surface dielectric barrier discharge generated by a perforated ceramic substrate in a configuration with the air-exposed electrode was investigated. The electrical characteristics (discharge power, peak, and average amplitude of current pulses) and optical characteristics (emission intensity) of the discharge were evaluated under various conditions of applied voltage (peak voltage 3–6 kV, frequency 200–2000 Hz), air flow rate (0.5–2.4 L/min), and air relative humidity (0%–80%). Temperature of ceramic substrate was also monitored. Statistical analysis of current pulses was also performed, and histograms of amplitudes of current pulses were calculated. The results showed that discharge characteristics strictly depend on given working conditions. The analysis of current pulses showed opposite trends in average overall number of positive and negative pulses with an increase of discharge power: number of positive current pulses gradually increased, while number of negative current pulses slightly decreased. The highest peak currents were found at 4 kV (1.8 W). With further increase of peak voltage, peak current decreased and beginning of detection of current pulses upon a rising (declining) slope of applied voltage was slightly shifted toward earlier times. At the highest applied peak voltage, pulses appeared even before polarity of applied voltage reversed. Therefore, we suppose that a residual charge accumulated on dielectric surface plays a crucial role in characteristics of the current pulses. Significant influence on current pulses and discharge emission intensity was also found with a change of air relative humidity, while the effect of air flow rate was found weaker.

Published under an exclusive license by AIP Publishing. https://doi.org/10.1063/5.0101496

I. INTRODUCTION

Dielectric barrier discharges (DBDs) have been investigated for many decades as one of the most promising nonthermal plasma (NTP) sources because of their simplicity, scalability, and the availability of reliable, efficient, and affordable power supplies.[1] They are defined as electrical discharges with electrode configuration consisting of dielectric material in the discharge region.[2] The role of dielectric is to limit the average current density in the gas, and thus, it acts as a series ballast resistor.[1] Principles and underlying physical phenomena of the DBDs have been well described and discussed in many review papers and textbooks.[3–9] Since 1857, when DBD was first used for the ozone generation,[10] the DBDs have become increasingly attractive, and nowadays, they are widely used in many applications, e.g., surface treatment,[11,12] air pollution control,[13] bio-decontamination,[14,15] air flow modification and control,[16,17] excimer lamps,[18] plasma displays,[19] ion source in analytical detection devices,[20] and so on.

According to electrode configuration, two basic types of DBD can be distinguished—volume and surface discharge. In the volume dielectric barrier discharges, one or both electrodes are covered by the dielectric barrier and the NTP forms in the gas space between them. In the surface dielectric barrier discharges (SDBDs), both electrodes are in direct contact with the same barrier and the NTP forms on the

dielectric surface.[2,21] At atmospheric pressure, the DBDs consist of numerous microdischarges (filaments) with number being proportional to the amplitude of the applied voltage. The current pulses (peaks) recorded by the oscilloscope are, indeed, the electrical signature of the microdischarges and are a measure of the transferred charge within discharge region.[8,22] Therefore, in-depth investigation of characteristics of the current pulses is very important.

SDBDs have been predominantly used for surface treatment applications and flow control in aerodynamic applications. For the applications of surface treatment of various materials, a diffuse coplanar surface barrier discharge (DCSBD) has a special position due to generation of a thin layer of NTP with a high-power density in a close vicinity of the treated surface.[23–25] In flow control applications, so-called plasma actuators usually based on SDBDs are commonly used.[16,17] They are typically composed of dielectric barrier and two electrodes placed on both its sides with symmetrical or asymmetrical pattern.

In the recent years, a special type of discharge so-called the multi-hollow SDBD has also been widely investigated. Within the literature, the discharge is also known as honeycomb DBD,[26] array of integrated coaxial micro-hollow DBD,[27–30] micro-hollow SDBD,[31] or array of micro-hollow cathode discharge.[32] The discharge is typically generated by a perforated ceramic substrate made of laminated ceramic sheets in two configurations. First configuration consists of two perforated parallel plate electrodes both embedded inside the ceramic, while the second configuration has one electrode embedded inside the ceramic and the other one printed on the ceramic surface (i.e., air-exposed electrode). Upon application of AC high voltage (HV) to the electrodes, the discharge is generated at the edge of each single hole (hollow), while the gas can pass through the holes. This type of discharge has an advantage of easy scalability, and it offers "grid-like" array geometry[27,30] suitable for flow control applications.[22,26,32] Moreover, the geometry enables efficient gas mixing with the NTP, what can possibly be used in many environmental applications, such as air pollution control. The discharge in both configurations has been already studied by many authors.

The first configuration of the multi-hollow SDBD with both electrodes embedded inside the ceramic has been investigated much more frequently. Physical characterization of the discharge was performed by many authors. Tachibana *et al.* performed the optical characterization of the discharge in He, Ar, and N_2 gases along with the evaluation of the production and spatiotemporal distribution of OH radicals produced by the discharge.[29] Optical characterization of the discharge in He and N_2 gases in a pressure range 20–100 kPa was also performed by Sakai *et al.*[28] and in N_2/NO gas mixtures by Shimizu *et al.*[33] Homola *et al.* used the optical emission spectroscopy (OES) in order to monitor rotational and vibrational temperatures of the discharge in ambient air.[31] Nayak *et al.* investigated the effect of gas flow rate and gas residence time on the discharge properties using highly time-resolved electrical and optical diagnostics.[27] They also studied the effect of gas flow rate and discharge power on the production of O_3 and $O_2(a^1\Delta_g)$ by the discharge.[34] Moreover, the applications of the multi-hollow SDBD with both electrodes embedded inside the ceramic have also been studied. Homola *et al.* studied the effects of duty cycle of applied voltage and air flow rate on O_3 production.[35] In other work, Homola *et al.* also investigated an influence of the discharge on the polycarbonate surfaces,[31] while Krumpolec *et al.* used the discharge

for fast cleaning and activation of silicon wafers.[36] Biomedical applications of the discharge were studied by several groups of authors.[30,37–40] Bacterial decontamination of various types of surfaces by the discharge was studied by Aboubakr *et al.*[30] and Kelar Tučeková *et al.*[37] Gebremical *et al.* investigated the effects of the discharge on physical quality and chemical and antioxidant properties of peanuts,[38,39] and Nayak *et al.* studied the effect of the discharge on inactivation of feline calcivirus.[40]

The second configuration of the multi-hollow SDBD with the one electrode embedded inside the ceramic and the other one printed on the ceramic surface has been studied only by a few authors. Benard *et al.* performed basic electrical and optical characterization of the discharge using high-resolution oscilloscope measurements and intensified charge-coupled device (ICCD) imaging.[22,26] The authors also investigated the electric wind produced by a single-hole discharge as well as influence of the discharge on a turbulent gas flow passing through the holes.[22,26] A special configuration of the double-stacked multi-hollow SDBD composed of four electrodes (two electrodes embedded inside the ceramic; two air-exposed electrodes) was studied by Elkholy *et al.*[32] In this work, the effects of the gas pressure and flow rate were investigated on discharge intensity by time-resolved optical emission spectroscopy measurements.

In contrast to the works of the above authors[22,26,32] in which the multi-hollow SDBD in configuration with the air-exposed electrode was studied, detailed characterization of electrical characteristics of the discharge under various operating conditions, to the best of our knowledge, is still missing. In addition, the evaluation of the discharge emission intensity under various conditions is also important as it represents a measure of concentration of reactive species generated by the discharge. Moreover, both electrical and optical characterization of the discharge is also crucial in respect to its eventual applications and their further optimization especially in ambient air conditions. Therefore, the main objective of our work, which distinguishes it from the other existing works, was to comprehensively investigate the "macroscopic" characteristics of the discharge (e.g., discharge power, properties of current pulses, emission intensity) that can be measured and analyzed relatively easily without a need of expensive experimental instruments and to address some interesting statistical aspects of multi-hollow SDBD. Variations of these characteristics were further investigated as a function of various operating conditions of applied voltage (3–6 kV at 200–2000 Hz), discharge power (1–5 W), air flow rate (0.5–2.4 L/min), and air relative humidity (RH) (0%–80%). In comparison with the works of other authors, this work for the first time presents how the properties of current pulses (amplitude, number) of the multi-hollow SDBD change with variations of basic operating conditions.

II. EXPERIMENTAL SETUP AND METHODS

The experimental setup is depicted in Fig. 1. The multi-hollow SDBD was generated by a perforated square ceramic substrate (Kyocera, KD-EB2B10) with the dimensions of 50 × 50 × 1 mm consisting of 170 holes (hollows) with an inner diameter of 1.5 mm [Figs. 2(a)–2(c)]. The distance between centers of two adjacent holes was 2.5 mm in one direction and 2.165 mm in the other direction. The substrate consisted of two electrodes made of Ni/Au alloy: one embedded inside the ceramic and the other one printed on the ceramic
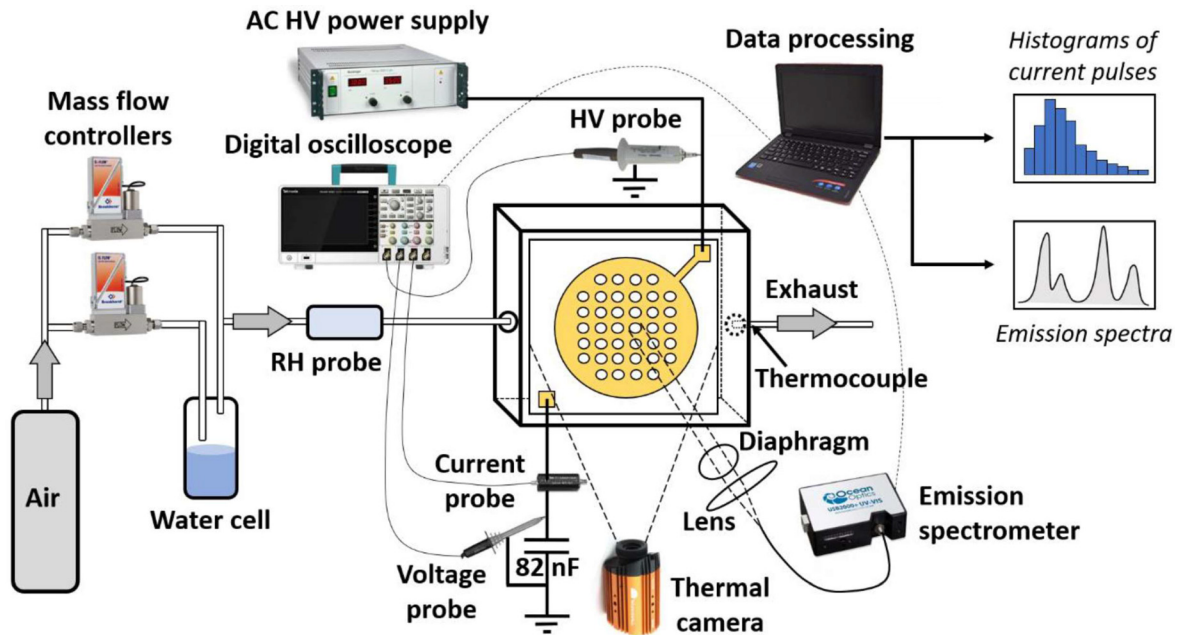
FIG. 1. Experimental setup.

surface (air-exposed electrode). The distance between the edge of the air-exposed electrode and the border of the corresponding hole was 0.2 mm [Fig. 2(a)]. The substrate was powered by AC HV power supply consisting of a function generator (GwInstek SFG-1013), a signal amplifier (Omnitronic PAP-350), and a HV transformer. The HV was connected to the air-exposed electrode, while the embedded electrode was grounded. Upon application of the AC HV, the discharge was generated at the edges (circumferences) of the holes [Figs. 2(a) and 2(c)]. The waveform of the applied AC HV was measured by the HV probe (Tektronix P6015A) and the discharge current by a current probe (Tektronix CT-1) both connected to a digital oscilloscope (Tektronix TBS2104; sample rate up to 1 GS/s; bandwidth 100 MHz) (Fig. 1). The power consumption of the discharge was evaluated using the method of Lissajous figures (also known as V–Q plots[2]) with an 82 nF capacitor and a voltage probe (Tektronix P2220). Optical characteristics of the discharge were measured through a quartz glass window and by using an optical emission spectroscopy (OES) system consisting of a dual-fiber optic spectrometer (Ocean Optics

SD2000), optic fiber, lens, and diaphragm. The OES system was adjusted to collect an emission from a single hole of the ceramic substrate with an integration time of 5 s. Photographs of the discharge were taken with a digital camera (Sony Alpha DSLR-A230) with manually adjustable aperture and exposure time. Synthetic (dry) air (purity 5.0) supplied from a pressure tank was used as a carrier gas, and its flow rate was controlled by mass flow controllers (Bronkhorst El-Flow Prestige FG-201CV). The air was alternatively enriched by water vapors by passing it through a water cell. The air RH was monitored by a capacitive humidity sensor (Arduino). Then, the air was led into the reactor chamber from the bottom side of ceramic substrate, it passed through the substrate holes, and it exited the substrate by its top side with the air-exposed electrode [Fig. 2(a)] and left the reactor chamber. Surface temperature of the ceramic substrate was monitored by infrared thermal camera (Workswell WIC2), and gas temperature was measured by a thermocouple placed at the outlet from the reactor chamber.
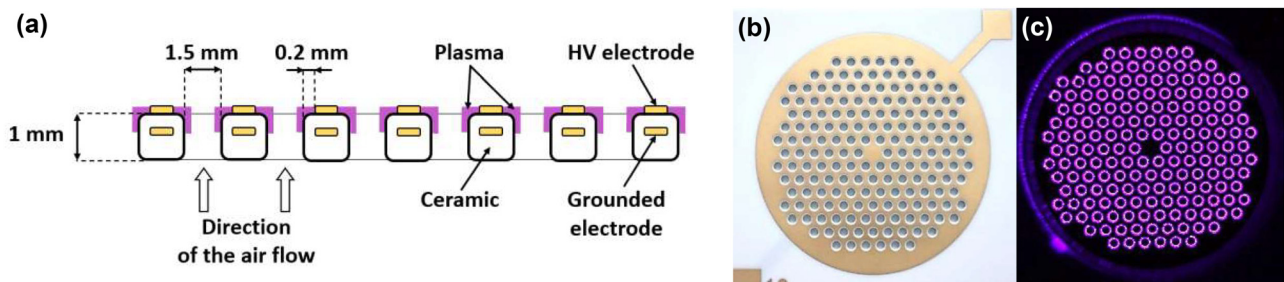

FIG. 2. [(a)–(c)] (a) Cross-sectional and (b) top view of the ceramic substrate; (c) photograph of multi-hollow SDBD (4 kV at 1 kHz) (Exposure time 3 s, f/5.6, ISO 400).

The multi-hollow SDBD was operated under various conditions of the applied voltage (peak voltage 3–6 kV, frequency 200–2000 Hz), air flow rate (0.5–2.4 L/min), and air RH (0%–80%). The effects of these parameters on electrical characteristics—discharge power, average amplitude (i.e., average current I_{avg}), maximum amplitude (i.e., peak current I_{max}), and number of current pulses and emission intensity of the discharge—were investigated. The peak current I_{max} was evaluated from the current waveforms and presented data represent its average values obtained during 30 min of discharge operation. The single-shot current waveforms were recorded by a digital oscilloscope using a sample rate of 250 MS/s that corresponds to a sample interval of 4 ns between two adjacent data points. A statistical analysis of the recorded current pulses was then performed and histograms of amplitudes of current pulses were calculated using a self-developed computer program. First, the program separated a capacitive component of the current waveform by applying the Fourier-transform method and also separated high-frequency noise signals. The calculated capacitive component of the current was further considered as a baseline (Fig. 3). Then, the program separated the pulses into positive and negative ones and counted them by checking all data points in one period of the applied voltage as follows: a data point was positively identified as a pulse when its amplitude (vertical distance of a data point from the baseline) was bigger than the amplitudes of two adjacent data points. If a peak of the pulse consisted of more than one data point of the same value, the pulse was counted as one. In some cases, overlapping pulses could also be found in the waveforms. If a data point between peaks of the adjacent overlapping pulses had lower value (i.e., lower amplitude) than the peaks, the pulses were counted as two. Otherwise, the pulse was counted as one. Finally, the histograms of amplitudes of the current pulses were calculated. The histograms were composed of several bins (intervals) of a 5 mA bin width, i.e., representing groups of pulses with amplitudes separated by 5 mA. The minimum amplitude of the pulse (i.e., height threshold) was set to 10 mA for both polarities. Data points with values below this threshold were not counted as they could be easily mistaken with a background electromagnetic noise and residual and random pulses due to inductance and capacitance of connecting cables (Fig. 3). The data presented in histograms represent average number of pulses during the positive and negative half-period of the applied voltage evaluated from ten independently recorded current waveforms. Finally, a distribution of current pulses in histograms bins also allowed for the calculation of their average amplitude, i.e., the current pulses in respective histograms bins

were sum up and divided by their overall number. The error bars of all presented data were calculated as standard deviations.

A gap voltage U_g is another important parameter for DBDs in general, and it can be calculated using the equation as follows:[2,41]

$$U_g(t) = V(t) - \frac{Q(t)}{c_{diel}},$$

where $V(t)$ is the voltage applied on the reactor, $Q(t)$ is the charge transferred by the discharge, and c_{diel} is the capacitance of the dielectric. The voltage $V(t)$ is measured by high-voltage probe, the charge $Q(t)$ can be determined from the voltage measurements on the capacitor, and the capacitance c_{diel} can be inferred from the Lissajous figures (slope of the line in V–Q plots during discharge active phase). The equation is based on the simplest DBD equivalent circuit that assumes a spatially uniform discharge. For this reason, U_g given by the above equation always represents an average over the DBD surface area and, thus, describes average properties of DBD resulting from large number of microdischarges.[41] In addition, a waveform of the gap voltage $U_g(t)$ also allows for determination of so-called burning voltage U_b (also known as discharge voltage[2]). It is defined as a certain threshold of gap voltage U_g when an inception of the discharge occurs. Determination of U_b from $U_g(t)$ can be applied if a "classical" approach (i.e., the simplest DBD equivalent circuit) is considered and the U_g is almost constant during discharge active phase (then $U_g \approx U_b$). The U_b can be also determined from Lissajous figures if their shape resembles an ideal parallelogram.[2]

III. RESULTS AND DISCUSSION
A. The effect of the applied voltage
1. Electrical and visual characteristics

The voltage and current waveforms of the multi-hollow SDBD at various peak voltages V_p (i.e., amplitudes of the applied voltage) are shown in Figs. 4(a)–4(d). By changing V_p, the current waveform changed significantly in terms of number and amplitude of current pulses. At V_p of 3 kV (at 1 kHz), the discharge started to form at the circumference of air-exposed electrode as well as at the edges of few holes of the ceramic substrate [Fig. 5(a)]. Upon increasing V_p from 3 to 4 kV, the discharge gradually started to form at the edges of all holes [Figs. 5(b) and 5(c)] and the number, peak current I_{max} as well as average current I_{avg} of the pulses substantially increased [Figs. 6(a) and 6(b)]. With further increase of V_p from 4 to 6 kV, the intensity of
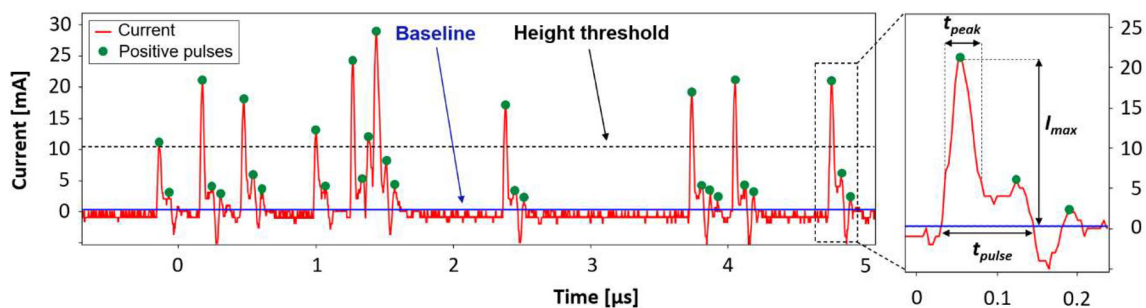

FIG. 3. Detail of recorded current waveform with marked baseline and height threshold. A detail of individual current pulse is also shown, where difference between t_{peak} and t_{pulse} is clearly visible.
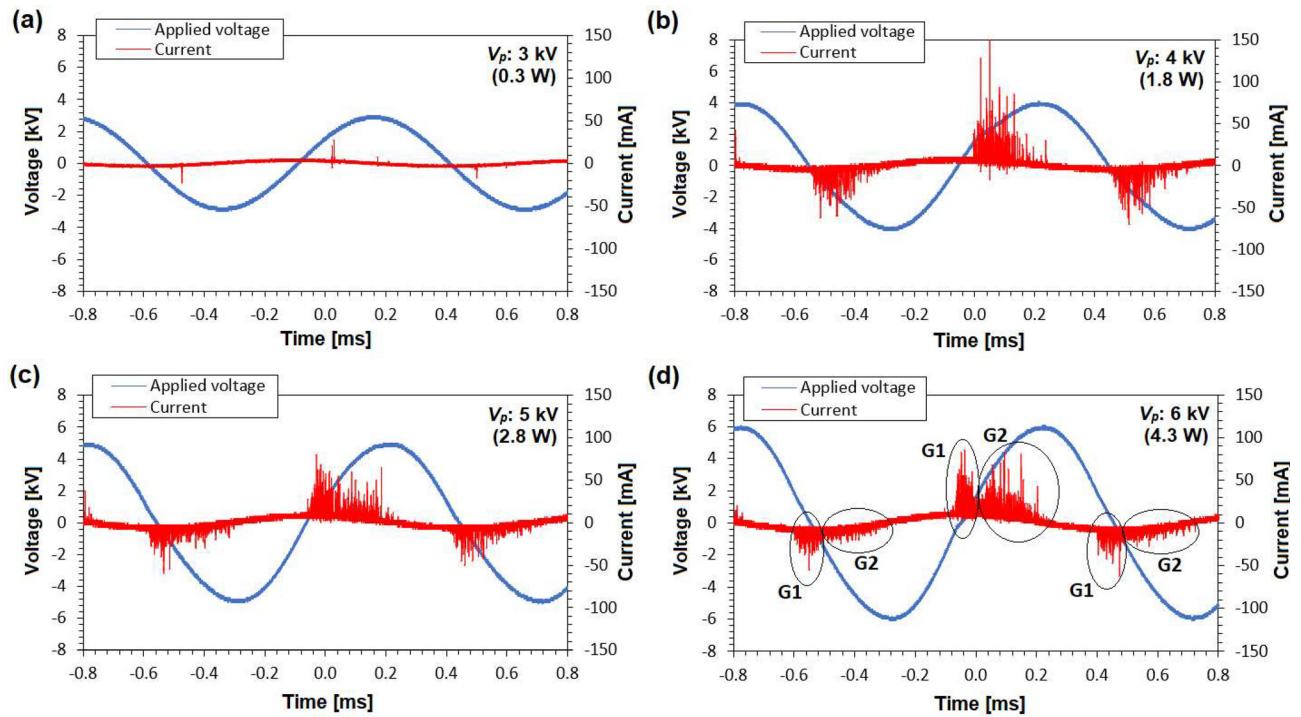
FIG. 4. [(a)–(d)] Applied voltage and current waveforms of multi-hollow SDBD at various peak voltages V_p: (a) 3 kV, (b) 4 kV, (c) 5 kV, and (d) 6 kV (dry air, 2.4 L/min, 1 kHz). The groups of pulses "G1" and "G2" are also denoted.
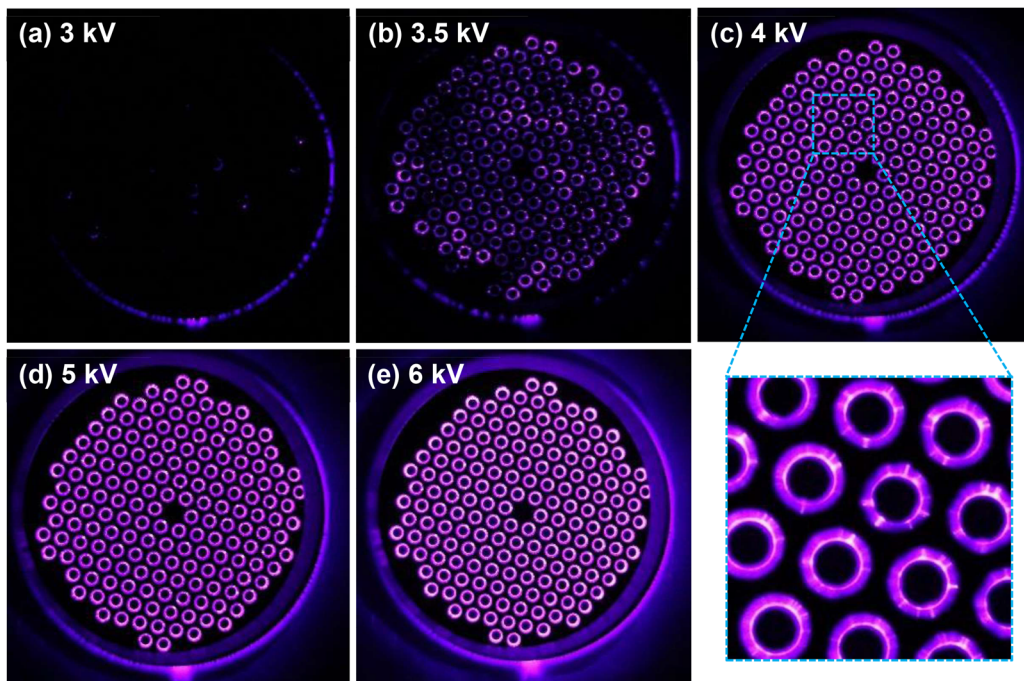

FIG. 5. [(a)–(e)] Photographs of multi-hollow SDBD at various peak voltages V_p (dry air, 2.4 L/min, 1 kHz) (Exposure time 1.6 s, f/5, ISO 800).
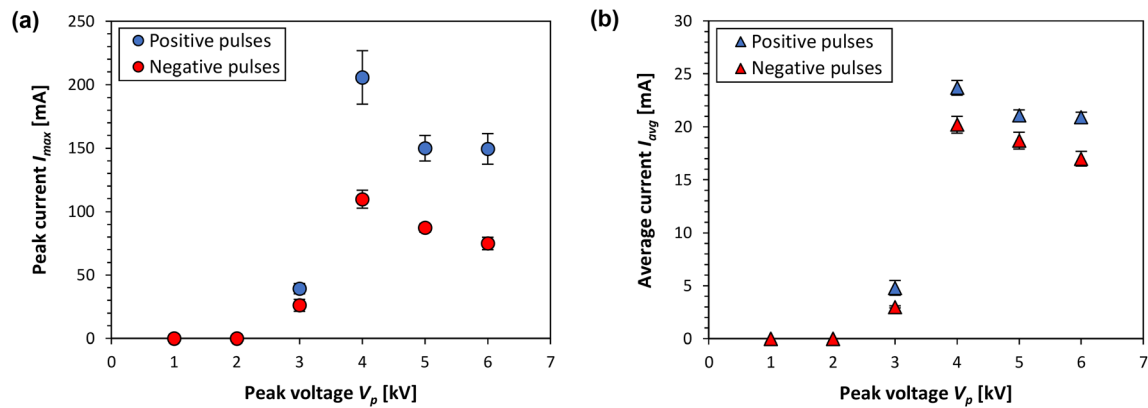
FIG. 6. [(a) and (b)] (a) Peak current I_{max} and (b) average current I_{avg} of both positive and negative current pulses as a function of peak voltage V_p (dry air, 2.4 L/min, 1 kHz).

the discharge further increased [Figs. 5(d) and 5(e)], number of current pulses increased too, whereas both I_{max} and I_{avg} slightly decreased [Figs. 6(a) and 6(b)]. A similar observation was reported by Nayak *et al.* who investigated the multi-hollow SDBD in the configuration with both electrodes embedded inside the ceramic.[34] They reported that with increasing the discharge power, the peak current I_{max} did not necessarily increase; however, more discharge events (i.e., microdischarges) within a half-period of the applied voltage were observed. Our results showed that both the highest positive and negative I_{max} were observed at V_p of 4 kV (206 and 110 mA, respectively), and with a further increase from 4 to 6 kV, I_{max} slightly decreased to 150 and 75 mA, respectively [Fig. 6(a)]. The I_{avg} of both positive and negative pulses followed the same trend as I_{max}: the highest values were observed at 4 kV (24 and 20 mA, respectively) followed by their slight decrease with an increase of V_p from 4 to 6 kV [Fig. 6(b)]. The measurements further showed that I_{max} as well as I_{avg} of positive pulses were always higher than that of negative pulses [Figs. 6(a) and 6(b)], what principally corresponds to the findings of Benard *et al.*[26]

The current waveforms further showed that at V_p of 4 kV (i.e., discharge power of 1.8 W), the first positive current pulses were detected at instantaneous applied voltage of approximately 1.5 kV, while the negative pulses around the point when AC HV crossed its zero value (i.e., passed through 0 kV) [Fig. 4(b)]. With further increase of V_p (and, thus, discharge power), a beginning of detection (i.e., onset) of current pulses upon a rising (declining) slope of applied voltage was slightly shifted toward earlier times [Figs. 4(c) and 4(d)]. Furthermore, at the highest applied V_p, the current pulses were detected even before polarity of the applied voltage reversed. The positive pulses began to precede the reversion of the polarity of the applied voltage from V_p of approximately 5.5 kV (3.8 W), while negative pulses from V_p of approximately 4.5 kV (2.5 W). This can be principally explained by the accumulation of surface charge on the dielectric during the previous half-period of the applied voltage. When local electric field induced by the residual surface charge reaches a sufficiently high intensity, an actual gap voltage can reach a burning (breakdown) voltage U_b even before the voltage polarity reverses.[2,42–44]

At V_p of 4 kV [Fig. 4(b)], the current waveform looks like a "common" DBD waveform, and there is only one "group" of current pulses in both polarities. At higher V_p of 5 and 6 kV [Figs. 4(c) and 4(d)], the residual surface charge started to play an important role.

In addition to the detection of current pulses before voltage polarity reversed, the current waveforms within one half-period of the applied voltage were split into two groups of pulses [denoted as G1 and G2 in Fig. 4(d) where this effect is evident]. The first group G1 involved the pulses that started to appear at the end of previous half-period, and their occurrence ended after the moment when AC HV passes through 0 kV. The second group G2 included positive (or negative) pulses that appeared during a rising (declining) phase of corresponding half-period until a moment when AC HV reached a peak value. In addition, the second group G2 is characterized by lower I_{max} and I_{avg} than first group G1. Similar effect of splitting the current waveform into two individual groups within one half-period of the applied voltage was also reported by Jahanbakhsh *et al.*[45] who worked with a simpler experimental arrangement (a barrier corona with a metal pin and a hemispherical dielectric-covered electrode powered by AC HV). A presence of two individual groups of current pulses within one half-period of the applied voltage is the result of differences in the volume and surface charge conditions before the microdischarges inception.[45] While the residual volume charges affect the streamer inception and its propagation in the discharge gap, the residual surface charges influence the surface streamer propagation. Since we worked with the SDBD arrangement without a defined discharge gap and where a charge transfer takes place just in a thin layer on the dielectric surface,[8] we suppose that just a residual surface charge on the dielectric plays a crucial role.

Another perspective on the splitting of current waveform into two group of pulses may be acquired from a waveform of the gap voltage $U_g(t)$ [Fig. 7(a)]. At the beginning of a positive half-period of the applied voltage, U_g increases. The increase of U_g is followed by a sudden drop and then by a further increase until U_g reaches a constant value [Fig. 7(a)]. A sudden drop of U_g corresponds to strong current pulses that belong to the first group of pulses G1 [Fig. 7(b)]. The microdischarges represented by the group G1 are influenced by the residual surface charge that remains from a previous half-period. In a case of positive pulses, there is a negative residual surface charge left by negative pulses and vice versa. Since microdischarges represented by the group G1 leave behind a charge of opposite polarity on the ceramic surface, initial conditions for subsequent microdischarges are considerably changed.[46] First positive group of pulses G1 leave behind a positive residual surface charge and vice versa. An electric field in the
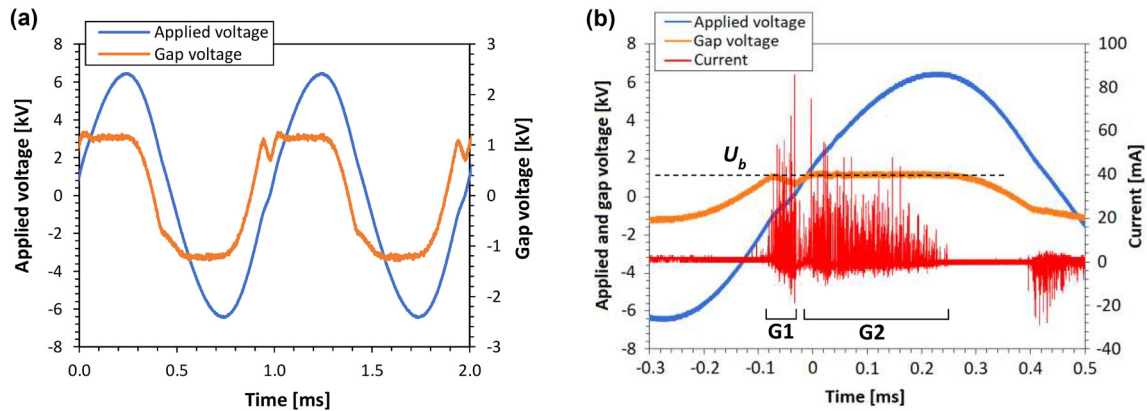
FIG. 7. [(a) and (b)] Applied voltage, gap voltage, and current waveforms (5 W, peak voltage V_p of 6.5 kV). Burning voltage U_b as well as groups of pulses G1 and G2 are also denoted.

discharge gap decreases and an instantaneous gap voltage U_g suddenly drops. However, the applied voltage further increases, gap voltage U_g starts to increase again until it reaches a constant value, so the microdischarges represented by the group G2 appear. Therefore, the microdischarges represented by the group G2 are affected by a residual surface charge that remains from microdischarges represented by the group G1. In other words, the initial conditions for successive discharge pulses are given by the charge distribution on the dielectric surface left after the preceding discharge pulses.[8] For this reason, we consider that the splitting of current waveforms may be ascribed to the change of a surface charge distribution within one half-period. In the negative half-period of the applied voltage, a situation is similar. Although no sudden drop is observed during an increase of negative gap voltage, its increase is slowed down in the moment when pulses of the group G1 appear. When microdischarges represented by the group G2 occur, U_g reaches a constant value. The constant value of U_g also allows for determination of burning voltage U_b. Since the Lissajous figures we obtained were very close to ideal parallelogram shape [Fig. 8(a)], U_b can be also determined from them. Both approaches of U_b determination gave us a value of approximately 1.2 kV for 5 W at peak voltage V_p of 6.5 kV.

The effect of residual surface charge accumulated from one half-period of the applied voltage to another half-period is also known as a memory effect that, among other things, facilitates a formation of microdischarges at the same location occupied by previous microdischarges.[5,9,42,43,46–48] Moreover, the accumulation of residual surface charge may also have an influence on other characteristics of the current pulses including their overall shape,[45] and the influence increases with an increase of peak voltage,[42] what we also observed. We further suppose that a change of surface charge distribution within one half-period may also be responsible for an observed decrease of I_{max} and I_{avg} with an increase of V_p above the value of 4 kV [Figs. 6(a) and 6(b)]. Shifting the onset of current pulses toward earlier times upon a rising (declining) slope of applied voltage caused an earlier accumulation of residual surface charge that subsequently decreases an intensity of electric field between the electrodes within a corresponding half-period. It affects the formation of subsequent microdischarges (current pulses) within the same half-period and decreases a charge transfer. Since the onset of current pulses shifts with an increase of V_p, we can, therefore, also expect a decrease of I_{max} and I_{avg}.
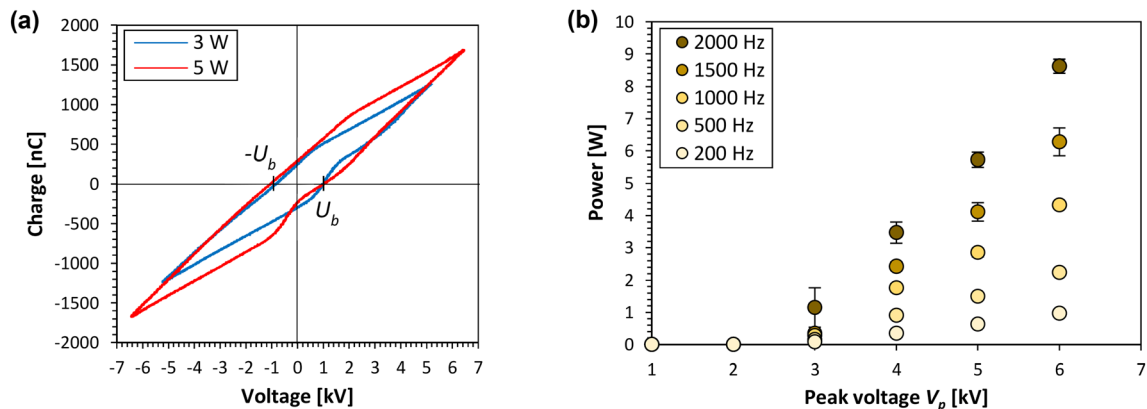

FIG. 8. [(a) and (b)] (a) Selected Lissajous figures with denoted burning voltage U_b for discharge power of 3 and 5 W; (b) discharge power as a function of peak voltage V_p at various frequencies of the applied voltage (dry air; 2.4 L/min).

2. Discharge power

Discharge power was evaluated using the method of Lissajous figures [Fig. 8(a)]. Figure 8(b) shows the discharge power as a function of peak voltage V_p at various frequencies of the applied voltage. The discharge power increased with frequency of the applied voltage and increased almost linearly with V_p. At V_p of 6 kV and a frequency of 500, 1000, and 2000 Hz, the discharge power was 2.2, 4.3, and 8.6 W, respectively. These results are comparable to those of other authors who studied the same type of discharge, i.e., the multi-hollow SDBD in configuration with the air-exposed electrode. For example, at the same V_p of 6 kV, Benard *et al.* reported discharge power of 1.8, 4, and 11 W at the frequency of 500, 1000, and 2000 Hz, respectively.[22] A fact that ceramic substrates they used were of a different geometry, dimensions, and number of holes can explain reported slightly different results. On the contrary to our observations, in their work, increase of discharge power with an increase of V_p did not show a linear trend.

3. Histograms of current pulses

The histograms of both positive and negative current pulses displaying their number vs their amplitude for given discharge power in a range of 1–5 W are presented in Figs. 9(a) and 9(b) with vertical logarithmic scales. The histograms show an average distribution of amplitudes of current pulses per half-period of the given applied voltage. They clearly indicate that the number of pulses and distribution of their amplitudes strictly depends on the discharge power as well as on the applied voltage polarity.

The results showed that number of positive pulses was always higher than negative ones [Figs. 9(a) and 9(b)]. Further, the distribution of amplitudes of the pulses in histograms showed that the number of pulses in a given bin usually decreased with an increase of the amplitude of the pulses. The most visible feature of histograms of positive pulses is an increase of number of pulses in respective bins with an increase of discharge power. This increase is more pronounced for pulses with amplitudes up to 60 mA [Fig. 9(a)]. On the contrary, histograms of negative pulses showed an opposite feature: a decrease of number of pulses with an increase of discharge power in respective bins especially for pulses with amplitudes in a range of 15–30 mA [Fig. 9(b)]. Consequently, the average overall number of positive pulses (>10 mA) substantially increased with an increase of discharge power (from approximately 117 ± 3 to 427 ± 10 pulses for 1 and 5 W, respectively), while the average overall number of negative pulses (>10 mA)
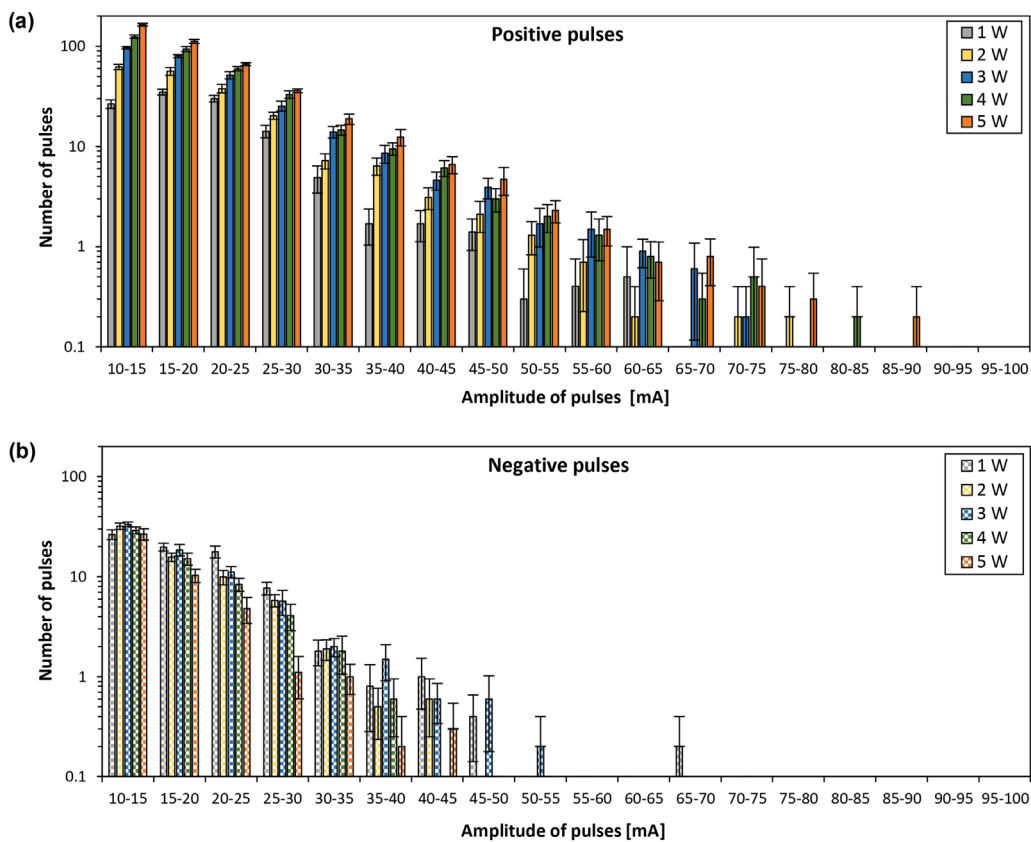

FIG. 9. [(a) and (b)] Histograms of amplitudes of (a) positive and (b) negative current pulses for various discharge powers 1–5 W (dry air, 2.4 L/min, 1 kHz). Data presented in histograms represent average number of pulses evaluated from ten independently recorded single-shot current waveforms.

slightly decreased (from approximately 76 ± 7 to 44 ± 6 pulses for 1 and 5 W, respectively). Our results are consistent with the findings of Benard et al.,[22,26] who also observed similar differences between characteristics of multi-hollow SDBD during positive and negative half-periods. During the positive half-period, more numerous current pulses with higher amplitudes were observed. On the other hand, during the negative half-period, smaller and less numerous current pulses were reported. Moreover, they also performed a fast ICCD imaging of the discharge and revealed that emission intensity of the discharge filaments during positive half-period was found three times higher than those during negative half-period.

When the applied voltage has a positive polarity (i.e., a positive half-period), the discharge pattern is composed of distinct (discrete) channels appearing on the dielectric surface, while with a negative polarity, a diffuse discharge area can be observed and the discharge is almost uniformly distributed in a certain area along the electrode.[8,49] In addition, a discharge extension (i.e., the length of the discharge area) is not only dependent on peak voltage but also on its polarity. Upon increasing the peak voltage, the discharge area is enlarged. Moreover, with a positive polarity of the applied voltage, an extension of the discharge channels is considerably larger than with a negative polarity.[8] Murata et al. attributed this "polarity effect" of microdischarges in DBDs to different mobility of electrons and ions accumulated on the dielectric surface within a corresponding half-period.[50] Therefore, considerable differences between obtained histograms of positive and negative pulses can reflect different discharge patterns during positive and negative half-periods.[8,51]

A similar statistical analysis of the current pulses of the SDBD was also performed by Laurentie et al.[51] They studied the current characteristics of SDBD plasma actuator composed of two electrodes mounted on both sides of dielectric sheet in two configurations: both electrodes exposed, or one electrode exposed, and the other one encapsulated using an epoxy resin. Their results obtained with an encapsulated grounded electrode (i.e., the configuration similar to ours) are consistent with our results. They also observed an increase of overall number of positive current pulses with an increase of V_p (i.e., discharge power) as well as a decrease of their number in histogram bins with an increase of their amplitude. In addition, an amplitude of positive pulses was found to be substantially higher than negative ones what also agrees with our findings. Other statistical analysis of the current pulses has also been performed for DSCBD,[48] plane-to-plane DBDs,[44,52–54] point-to-plane DBD,[55] cylindrical DBD,[56] or cylinder-tip to dielectric plate DBD.[57] In contrast to our results, histogram analysis of current pulses performed by Čech et al. using a DCSBD,[48] Jidenko et al. using a plane-to-plane DBD,[44] and Petit et al. using a point-to-plane DBD[55] showed a shift of maximum number of pulses from their lower to higher amplitudes. The difference can be probably attributed to different discharge reactor arrangements that have been investigated (geometry and position of electrodes, device size, electrode materials, etc.), so only a rough comparison is possible. The most detailed statistical investigation of the current pulses was conducted by Jahanbakhsh et al. for a relatively simple arrangement of barrier corona with a metal pin and a hemispherical dielectric-covered electrode powered by AC HV.[42,45] Apart from electrical measurements, the other techniques they used included time-correlated single photon counting and ICCD imaging. Their detailed investigation revealed different types of microdischarges that may occur. They further

confirmed strong dependence of microdischarges on their onset (inception time and position), that is, related to the discharge activity in the previous half-period of the applied voltage.

As was already mentioned, the analysis of current pulses was based on current waveforms recorded by the oscilloscope using a sample rate of 250 MS/s that corresponds to a sample interval of 4 ns. The used sample rate could potentially lead to certain imperfections (deviations) in recording the exact shape of the pulses. A more accurate reconstruction of the pulses shape would require a sample interval around 1 ns at least. However, since a typical length (duration) of a current pulse t_{pulse} was $\sim$100–120 ns and a typical length of its main peak t_{peak} was $\sim$40–50 ns (Fig. 3), we consider that the used sample rate (sample interval) was good enough to acquire an individual current pulse with a sufficient number of data points. Another deviation in number of pulses could result from using the height threshold parameter that was used to ignore a noise. Too low pulses with amplitudes below this threshold, thus, were not counted meaning that not every single microdischarge could be measured. Therefore, presented numbers of pulses do not represent an exact number of microdischarges; however, we believe that the calculated and presented data can be still demonstrative.

4. Optical characteristics

The OES measurements of the multi-hollow SDBD were performed along with the electrical measurements. In the obtained spectra, emission bands corresponding to molecular nitrogen significantly dominated in all tested conditions. Namely, in the UV region, the N_2 second positive system (300–400 nm) with a maximum at 337 nm dominated, while in VIS region, the N_2 first positive system of very low intensity occurred (650–1000 nm). The OES of multi-hollow SDBD in configuration with both electrodes embedded inside the ceramic was also carried out by Homola et al.[31] Moreover, many authors conducted very precise time-resolved optical measurements of the multi-hollow SDBD in various configurations using ICCD cameras.[27–29,32,33] In addition to the N_2 second positive system, traces of N_2^+ first negative system[28,29,33] or NOγ system[27] were also observed while operating the discharge in air-like mixtures using a higher frequency of the applied voltage ($>$20 kHz) than we worked with.

Figure 10 depicts a dependence of discharge emission intensity on discharge power and frequency of the applied voltage. A change in the emission intensity was evaluated based on 0–0 spectral band (337 nm) of N_2 second positive system. The emission intensity linearly increased with an increase of discharge power for a given frequency of the applied voltage, and it also more or less increased with an increase of frequency for a given discharge power. The results clearly reflect an increase of N_2 electronic excitation with an increase of frequency. As can be seen in Fig. 10, for low discharge power in a range of 1–1.5 W, the highest emission intensity was obtained for the lowest frequency of 500 Hz. This was caused by an inhomogeneous ignition of the discharge at the edges of holes of ceramic substrate. At such low discharge power, the discharge was not fully distributed in each hole of the ceramic substrate. Since we detected a light signal only from a single hole of the ceramic substrate, the inhomogeneous ignition of the discharge in the holes could cause the observed differences. When the discharge power was higher ($>$2 W), the discharge was fully developed and generated at the edges of each hole of the substrate and the emission intensity showed a clear dependence on frequency of the applied
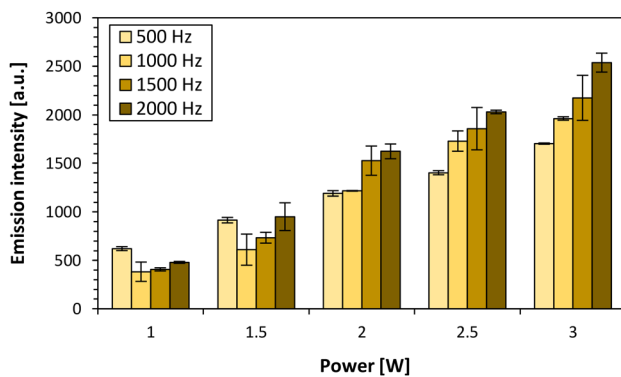
FIG. 10. Emission intensity of the discharge as a function of discharge power and frequency of the applied voltage (dry air, 1 L/min).

voltage. The results are consistent with the results of Abdelaziz et al.,[58] who observed an increase of emission intensity of symmetrical SDBD plasma actuator with an increase of frequency at the constant peak voltage V_p.

B. The effect of the air flow rate

By varying the gas flow rate, one can control a gas residence time in a zone of generated plasma. This has a direct impact on gas and substrate heating, residual humidity, residence time of charge carriers and, especially, on discharge chemical activity due to strong dependence of concentrations of excited and reactive species on gas flow rates.[27,59] Nevertheless, the gas flow rate cannot directly influence the properties of individual microdischarges (i.e., their ignition and development) due to very different time scales: while discharge formation occurs in a range from ps to μs, the flow dynamics applies from ms to s. More specifically, for our experimental conditions, a residence time of the air inside the holes (hollows) of ceramic substrate, i.e., in a plasma, was estimated as follows: 36.5, 18, and 7.5 ms for air flow rate of 0.5, 1, and 2.4 L/min, respectively. Therefore, the only processes that can be affected by the used gas flow rate are the diffusion and recombination of neutral and charged particles that take place within μs and ms. Consequently, the gas flow rate has only an impact on conditions prior to the breakdown itself meaning that it changes the concentration and distribution of residual volume charges from previous microdischarges (i.e., volume pre-ionization).[59] From a macroscopic point of view, residual volume charges can be moved (transported) and redistributed by flowing gas, thus, influencing ignition and development of microdischarges.[42,47] As a result, variation of air flow rate can influence the plasma characteristics[60] or even change the pattern (mode) of the DBD.[61]

1. Electrical characteristics

The effect of the air flow rate (0.5, 1, and 2.4 L/min) was investigated on electrical properties of the discharge (discharge power, histograms, number, and amplitudes of current pulses) for constant discharge power of 3 W and frequency of the applied voltage of 1 kHz. The results showed that the effect of air flow rate on discharge power at a given applied voltage is very small and, to some extent, can be neglected. Dependence of both peak current I_{max} and average current I_{avg} on the air flow rate was found weak as they only slightly increased

with an increase of air flow rate. For example, I_{avg} of positive pulses increased from 18 to 20 mA, while for negative pulses, it increased from 16 to 18 mA for an increase of the air flow rate from 0.5 to 2.4 L/min, and for a given discharge power of 3 W, respectively.

The histogram analysis of current pulses for various air flow rates for a constant discharge power was also performed and confirmed that the highest amplitudes of current pulses occurred at the highest tested flow rate (2.4 L/min) [Figs. 11(a) and 11(b)]. Moreover, the effect of air flow rate was found stronger on negative rather than positive pulses. There was almost no change in average number of positive pulses (>10 mA), whereas average number of negative pulses (>10 mA) considerably increased upon increasing the air flow rate. These results are in agreement with the results of Höft et al.[59] They also observed an increase of peak current I_{max} in the DBD reactor with an increasing gas flow rate. As was already mentioned, the residual surface charge plays quite an important role in generation of the multi-hollow SDBD. Although the residual surface charge, in contrast to residual volume charge, is not expected to be directly influenced by the gas flow rate, it can be affected indirectly. Besides an increase of peak current I_{max}, Höft et al. also observed an increase of breakdown voltage with an increase of gas flow rate, i.e., a beginning of the discharge formation upon a rising slope of HV pulse was slightly delayed.[59] A breakdown delay for higher air flow rates was also observed by Nayak et al. who worked with the multi-hollow SDBD in configuration with both electrodes embedded inside the ceramic.[27] This effect was ascribed to a removal of charges from the discharge region before a new breakdown occurs. However, Jidenko et al. further stated that higher gas flow rate can increase the extension of the charges along the dielectric surface what may eventually lead to stronger electric field during the development of next discharge.[44] Therefore, a change of breakdown conditions upon changing a gas flow rate may affect an accumulation of surface residual charge and also the amplitudes of current pulses.

2. Optical characteristics

The effect of air flow rate on emission intensity of the discharge was also investigated (Fig. 12). We found that emission intensity decreased with an increase of air flow rate for a given discharge power. On the other hand, an increase of a gas flow rate resulted in a slight increase of maximum and average amplitudes of current pulses as well as number of pulses. Thus, one may expect that more numerous and more intense microdischarges occur and higher production of reactive species along with higher discharge emission intensity would be observed. However, the results showed completely opposite trend as emission intensity clearly decreased with an increase of air flow rate (Fig. 12). It means that the explanation of results is not straightforward and other more dominant factors must be considered. Upon increasing the air flow rate, the gas residence time in a discharge region decreases. Because of that, the number of excited species per unit of a gas volume actually decreases, and thus, it results in lower emission intensity. The same results were observed by other authors dealing with multi-hollow SDBD.[28,31,32,34] Since a decrease of air flow rate for a given discharge power results in an increase of discharge energy deposited per gas volume (i.e., energy density), the discharge emission intensity increased with its increase (Fig. 12). Elkholy et al. compared the emission intensity of the discharge with
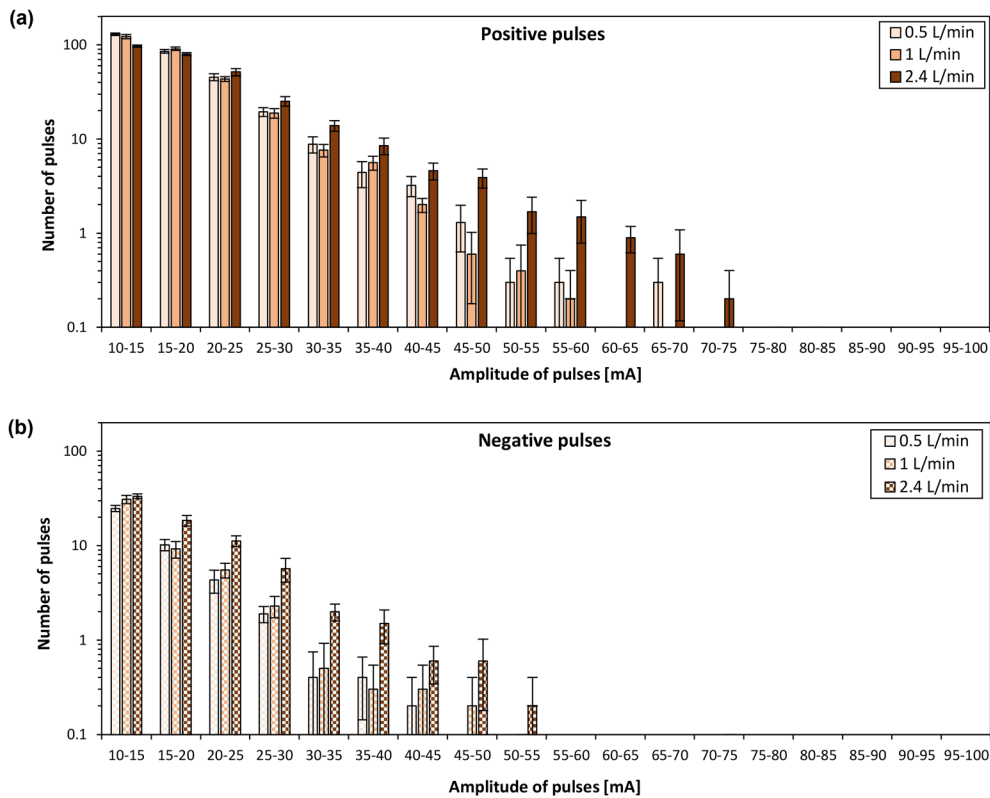
FIG. 11. [(a) and (b)] Histograms of amplitudes of (a) positive and (b) negative current pulses for various air flow rates (0.5, 1, and 2.4 L/min) (3 W, dry air, 1 kHz).

and without the air flow.[32] They reported that in a still air the discharge ionizes the same volume of gas increasing ionization level in the discharge region. When the air flow increases, discharge region is supplied with a fresh air causing a decrease of ionization level and, thus, the decrease of discharge emission intensity.

3. Temperature measurements

In addition to electrical and optical characterization of the discharge, gas and surface temperatures are other important parameters determining utilization of the discharge for eventual applications. The heating of the ceramic substrate during discharge operation is caused by dielectric losses in the material.[62] The heating of a gas passing through the holes of the ceramic substrate is caused by convective transport of heat from the dielectric as well as by an action of plasma itself.[62,63] We monitored the surface temperature as a function of discharge power and air flow rate (Fig. 13). The surface temperature increased with an increase of discharge power and slightly decreased with an increase of air flow rate. However, we found that a difference between surface temperatures obtained for the lowest (0.5 L/min) and highest tested air flow rate (2.4 L/min) for all tested discharge powers is relatively small
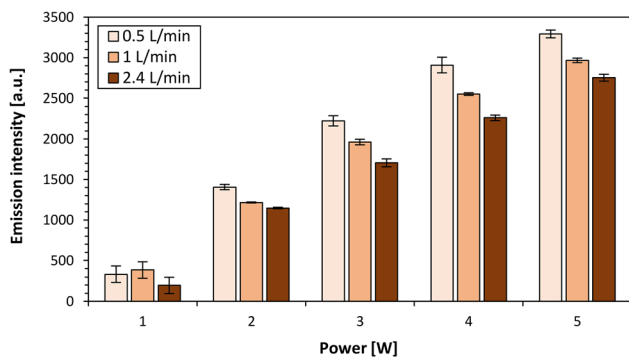

FIG. 12. Emission intensity of the discharge as a function of discharge power and air flow rate (dry air, 1 kHz).
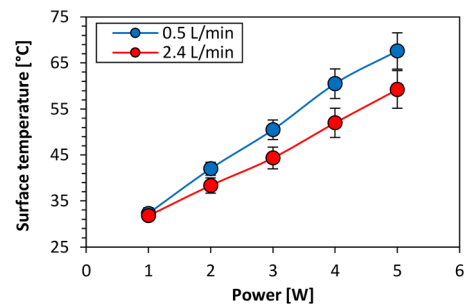

FIG. 13. Surface temperature of the ceramic substrate as a function of discharge power for two air flow rates (0.5 and 2.4 L/min).

(Fig. 13). The temperature can affect a surface conductivity of the dielectric that may further lead to modification of charges distribution on the dielectric surface.[44] Thus, the influence of temperature may also contribute, to some extent, to changes in the evaluated characteristics of the current pulses.

Measurements of gas temperature at the outlet of the reactor chamber showed similar results compared to surface temperature. The gas temperature increased with an increase of discharge power and slightly decreased with an increase of air flow rate. The maximum gas temperature we obtained was approximately 70 °C (5 W, 0.5 L/min), which is almost identical to maximum surface temperature we measured on the substrate. This is a reasonable result as all measurements were performed after substantially a long time of discharge operation, so we could assume steady-state conditions when surface and gas temperatures were approximately the same.[64]

C. The effect of the air relative humidity

Many sources of the NTP are usually operated in ambient air conditions that always include some humidity. Therefore, an effect of air humidity on discharge properties must be known and examined. An extensive research has been done in this field and showed that a presence of humidity (i.e., water molecules) has substantial effect on discharge formation, its properties, and behavior. First, the humidity influences the physical processes from various aspects. It affects a distribution of electric field,[65,66] a mobility of charge carriers,[67] a microdischarge intensity,[7] and a power loss in dielectric material.[68] It further reduces surface resistance of dielectric due to water adsorption[69] and total charged transfer per half-period of the applied voltage.[68,69] The humidity may also decrease the peak current of the discharge;[70] it modifies a charge distribution along the dielectric surface creating spatial charge inhomogeneities and may promote a formation of discrete microdischarges at preferred locations.[71] This, in turn, can lead to decrease in a number of microdischarges[70] and, thus, reduction of plasma volume within the reactor.[69] Second, the humidity also significantly affects and alters the plasma chemistry.[72] An increase of humidity can lead to formation of water negative ions due to electronegativity of water molecules[68] as well as to formation of water clusters.[73,74]

In the available literature, the effect of humidity on the discharges has been extensively investigated by several authors.[69,75,76] However, their conclusions are sometimes inconsistent, i.e., results of some authors are contradictory to results of other authors. Indeed, the effect of humidity on the discharges is very complex as it comprises many physical and chemical aspects. Therefore, an actual effect of humidity on the discharges depends on given working conditions (e.g., gas mixture, temperature, dielectric material, etc.) and the type of discharge.

1. Electrical characteristics

The effect of air RH on characteristics of current pulses was studied for constant discharge power of 3 W, frequency of the applied voltage of 1 kHz, and gas flow rate of 2.4 L/min. The experiments were performed at atmospheric pressure, constant room temperature of approximately 22 °C, and air RH levels of 20%, 40%, 60%, and 80%, so the absolute humidity of the air (water content) was 3.9, 7.8, 11.7, and 15.6 g/m³, respectively.

The results showed that the average current I_{avg} of both positive and negative pulses slightly increased with an increase of air RH. For positive pulses, it increased from approximately 20 to 27 mA, while for negative pulses, it increased from approximately 18 to 24 mA upon increasing the air RH from 0% to 80%, respectively. On the contrary, a variation of both positive and negative peak currents I_{max} with air RH showed more complicated trends. More specifically, with an increase of air RH from 0% to 40%, I_{max} of positive pulses first decreased from approximately 100–120 to 77 mA. However, with a further increase of air RH from 40% to 80%, I_{max} of positive pulses substantially increased from approximately 77 to 170 mA. In contrast to the positive, I_{max} of negative pulses showed a gradual increase from approximately 80 to 160 mA for air RH of 0% and 80%, respectively. We suppose that differences between the results obtained for positive and negative pulses can be again attributed to different discharge patterns during positive and negative half-period of the applied voltage.[77]

The effect of air RH on characteristics of current pulses in DBDs has also been studied by other authors who obtained diverse results. For example, Benard et al. observed a decrease of positive and increase of negative peak current I_{max} with an increase of air RH for SDBD plasma actuator.[77] Abdelaziz et al. observed a decrease of both positive and negative I_{max} of SDBD with an increase of air RH,[68] while Falkenstein and Coogan observed a completely opposite trend, i.e., an increase of both positive and negative I_{max} of DBD.[69] Here, it must be noted that the measurements performed by Benard et al., Abdelaziz et al. and Falkenstein and Coogan were made at a constant applied voltage. However, our measurements were carried out for a constant discharge power, i.e., the peak voltage V_p was accordingly set to get a given discharge power (3 W). Therefore, only a rough comparison of the results is possible. Falkenstein and Coogan further reported that under their experimental conditions, the dominant effect of humidity in a gas is not the electronegativity of water molecules, but its effect rather lies on the reducing of surface resistance of the dielectric, as water is adsorbed onto its surface.[78] Consequently, although the total transferred charge per half-period of the applied voltage was observed to decrease upon increasing a humidity content, the mean transferred charge of the single microdischarge increased resulting in fewer, but more intense current pulses.[69] This partially corresponds to our results especially for positive pulses whose number decreased (presented later) and their average amplitudes increased with an increase of air RH. However, as we described above, I_{max} of positive pulses showed a non-trivial trend upon increasing the air RH suggesting that not only reduction of surface resistance of the dielectric, but also other factors must be involved. Fouad and Elhazek numerically and experimentally investigated an effect of air humidity on positive corona discharge.[79] Although the authors studied a different type of discharge, mechanisms of positive corona discharge formation are somewhat similar to mechanisms of DBD formation during a positive half-period of the applied voltage. They reported a variation of ionization processes with an increase of air RH: upon its increase from 20% to 40%, the ionization processes were found to be less intense, while with further increase of air RH from 60% to 80%, more ionization took place. The authors suggested that a variation of the ionization zone length along with number of produced photoelectrons and their distribution within the ionization zone could be responsible for the obtained results. These results may principally correspond with our results of positive

peak current I_{max} which first decreased up to air RH of 40% and then it increased.

Histogram analysis of current pulses at various air RHs and a constant discharge power of 3 W was also carried out and confirmed a different effect of air RH on positive and negative pulses [Figs. 14(a) and 14(b)]. Similar to dry air, positive pulses were found to be more numerous than negative ones for all tested humidity levels. Variation of the average overall number of pulses with an increase of air RH was found, however, different. With an increase of air RH from 0% to 80%, a number of positive pulses (>10 mA) decreased from approximately 297 ± 8 to 202 ± 5, while a number of negative pulses (>10 mA) increased from approximately 69 ± 8 to 168 ± 8, respectively. The same trends for positive and negative pulses with an increase of air RH were also obtained by Abdelaziz et al. who investigated the characteristics of surface DBD.[68] Although they clearly showed that the air RH has significant effects on electrical characteristics of the discharge, the underlying mechanisms explaining the observed results still remain a matter for consideration.

Unlike the histogram of negative pulses [Fig. 14(b)] that showed an increase of pulses number for all their amplitudes, the histogram of positive pulses [Fig. 14(a)] demonstrated a more complicated trend with an increase of air RH. A different trend was found for a group of pulses with amplitude <25 mA in comparison with a group of pulses with an amplitude >45 mA. While number of pulses below 25 mA

decreased, a number of pulses above 45 mA more or less increased with an increase of air RH. Consequently, the average amplitude I_{avg} of positive pulses increased. These results principally correspond with findings of Falkenstein and Coogan who reported that fewer, but more intense positive current pulses of DBD occurred with an increase of air humidity.[69] Moreover, such a significant change of distribution of positive pulses amplitudes in histograms may also be related to a change of discharge pattern (mode) with a change of humidity. Wicks and Thomas worked with an SDBD actuator and observed a transition from glow discharge to filamentary discharge when air RH increased from 40% to 75% at a constant applied voltage.[71] They suggested that this effect is probably associated with a humidity-induced modification of the charge distribution on the dielectric surface resulting in spatial charge inhomogeneity what promotes discrete microdischarges formation. The same effect was also observed by Koo et al. for radio frequency-powered surface DBD.[80]

Nevertheless, distinct results obtained by the aforementioned authors and associated discussions presented above suggest that the effect of humidity on electrical characteristics of DBDs and related discharges is not trivial and probably depends on many factors. Therefore, we suppose that the humidity effects should be further examined with respect to type and geometry of the discharge, type of dielectric, gas mixture, and other experimental conditions.
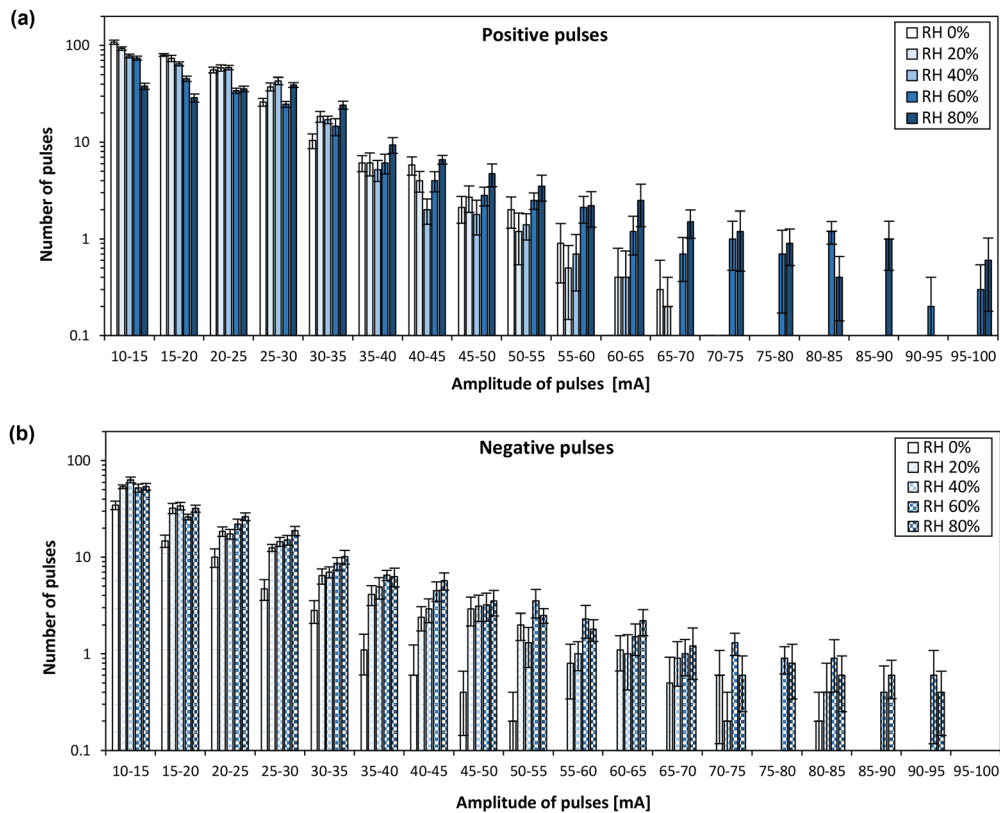

FIG. 14. [(a) and (b)] Histograms of amplitudes of (a) positive and (b) negative current pulses for various air relative humidities (0%–80%) (3 W, 2.4 L/min, 1 kHz).

2. Optical characteristics

Optical characterization in terms of discharge emission intensity was also evaluated as a function of air RH. Results showed that a dependence of discharge emission intensity on air RH is different for low and high discharge powers (Fig. 15): for discharge powers in a range of 1–3 W, the emission intensity significantly decreased with an increase of air RH, while for the highest tested discharge power of 5 W, the emission intensity was almost the same regardless of the air RH. In other words, the dependence of discharge emission intensity on air RH weakens upon increasing the discharge power. These results can be associated with a fact that in dry air and at low humidity levels, the discharge was stable and was almost homogeneously distributed in all holes of the ceramic substrate for a given discharge power. With increasing air RH, the discharge became less stable, and particularly for low discharge powers (1–2 W), it formed preferentially only in few holes. Homogeneous and fully developed discharge at the edges of all holes at higher air RH ($>60\%$) was obtained only for higher discharge powers (>3 W) and after a certain time of discharge operation (>10 min).

In addition, a decrease of emission intensity with increasing of air RH can also be attributed to a decrease of concentration of nitrogen excited species whose emission dominated in the emission spectra. Decrease of their concentration is probably due to faster vibration-to-vibration energy transfer of N_2–H_2O systems in humid environments,[81] and this effect seems to be more pronounced for discharge powers below 3 W. Decrease of emission intensity of the SDBD with an increase of air RH was also observed by Abdelaziz et al.[68] On the other hand, Tučeková et al. investigated the DCSBD and reported more complicated dependence of its emission intensity on air RH: first, it increased with the air RH from $<1\%$ to 50%, but with further increase to 85%, it dropped down even below the obtained value at air RH of $<1\%$.[82]

IV. CONCLUSION

The surface dielectric barrier discharges represent very promising nonthermal plasma sources due to their simplicity, low weight, and ergonomics. They are commonly used for surface processing of materials, and also for flow control, biomedical and environmental applications. In order 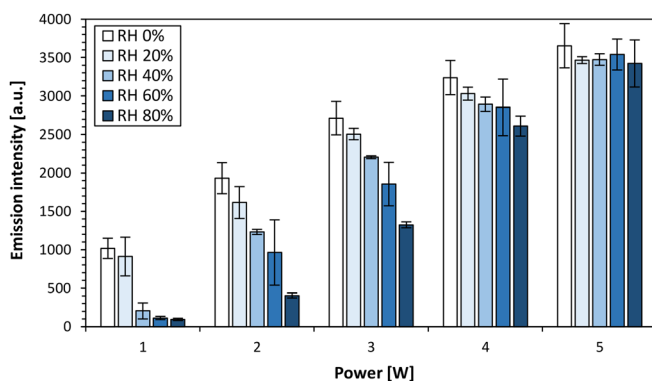to effectively employ the discharges for any application, their detailed characterization must be performed especially under ambient air operating conditions. This work presents the "macroscopic" electrical and optical characteristics of the special multi-hollow surface dielectric barrier discharge generated by a perforated ceramic substrate in a configuration with the air-exposed electrode. Properties of current pulses (maximum and average amplitudes) along with discharge emission intensity were evaluated under various conditions of applied voltage, air flow rate, and air relative humidity. The statistical analysis of current pulses was also performed and histograms of amplitudes of current pulses were calculated. In addition, the heating of surface of the ceramic substrate during discharge operation was monitored. Gas temperature at the outlet from the reactor chamber was also measured.

The result showed a strong dependence of both electrical and optical discharge characteristics on working conditions. Discharge emission intensity was found to increase with an increase of frequency of the applied voltage, and to decrease with an increase of air flow rate and relative humidity. With an increase of peak voltage (discharge power), histograms of amplitudes of current pulses showed an opposite trend for positive and negative pulses. While the average number of positive pulses substantially increased, the average number of negative pulses slightly decreased. The highest peak currents (approximately 206 mA for positive and 110 mA for negative pulses) were found at 4 kV (1.8 W). With further increase of peak voltage, the peak currents decreased and the onset of current pulses upon a rising (declining) slope of applied voltage was slightly shifted toward earlier times. When a maximum peak voltage was applied, the pulses appeared even before polarity of applied voltage reversed. This is due to the accumulation of surface charge on the dielectric during the previous half-period of the applied voltage. In addition, a splitting of current waveforms into two groups of pulses within one half-period of the applied voltage was also observed. We consider that this effect may be ascribed to the change of a surface charge distribution within one half-period.

The effect of air flow rate on characteristics of current pulses and distribution of their amplitudes in calculated histograms was found weaker than the effect of discharge power and air relative humidity. Both maximum and average amplitudes of current pulses increased very slightly with an increase of air flow rate for a given discharge power. We suppose that a change of breakdown conditions upon changing a gas flow rate may affect the accumulation of surface residual charge and, hence, the amplitudes of current pulses. The temperature measurements showed that surface and gas temperatures increased with an increase of discharge power and slightly decreased with an increase of air flow rate. The maximum surface and gas temperatures we obtained were almost identical (up to 70 °C).

The effect of air relative humidity on the discharge was found even more pronounced. The histogram of positive pulses showed a different trend for the pulses with amplitude below 25 mA and the pulses with amplitude above 45 mA. While number of pulses below 25 mA decreased, a number of pulses above 45 mA more or less increased with an increase of air relative humidity. On the contrary, a number of negative pulses increased with an increase of air relative humidity regardless of their amplitude. Consequently, an increase of air relative humidity caused an increase of the average amplitude of both positive and negative pulses. The results can be principally attributed to different mechanisms governing discharge formation during positive and

FIG. 15. Emission intensity of the discharge as a function of discharge power and air relative humidity (1 L/min; 1 kHz).

negative half-period of the applied voltage. In addition, various effects arising from an increase of air relative humidity can be also considered, including reduction of surface dielectric resistance, change of the charge distribution on the dielectric surface, variation in ionization processes, and so on. However, determining the exact underlying mechanisms and dominant effects still remains a matter for consideration.

Finally, the results showed that the obtained "macroscopic" results and characteristics (e.g., the splitting of current waveforms into two groups of pulses) can be, at least partially, explained by "microscopic" results (e.g., measurements of surface charge deposition) obtained by other authors. We may also conclude that the results are representative and can provide a good starting point for future waveform-based analysis of current pulses for various discharges. The characterization of the discharge under ambient air operating conditions is crucial for its optimal operation as well as for its eventual employment in various potential applications.

ACKNOWLEDGMENTS

AUTHOR DECLARATIONS
Conflict of Interest

The authors have no conflicts to disclose.

Author Contributions

Richard Cimerman: Conceptualization (equal); Data curation (equal); Formal analysis (equal); Investigation (equal); Methodology (equal); Supervision (equal); Writing %– original draft (equal); Writing – review & editing (equal). **Emanuel Maťaš:** Data curation (supporting); Investigation (supporting). **Matej Sárený:** Software (lead). **Karol Hensel:** Funding acquisition (lead); Methodology (equal); Resources (lead); Supervision (equal); Writing – review & editing (equal).

DATA AVAILABILITY

The data that support the findings of this study are available from the corresponding author upon reasonable request.

REFERENCES

[1] U. Kogelschatz, Plasma Chem. Plasma Process. **23**, 1 (2003).
[2] R. Brandenburg, Plasma Sources Sci. Technol. **26**, 053001 (2017).
[3] U. Kogelschatz, B. Eliasson, and W. Egli, J. Phys. IV Colloq. **7**, 7 (1997).
[4] U. Kogelschatz, IEEE Trans. Plasma Sci. **30**, 1400 (2002).
[5] A. Fridman, A. Chirokov, and A. Gutsol, J. Phys. D: Appl. Phys. **38**, R1 (2005).
[6] V. G. Samoilovich, V. I. Gibalov, and K. V. Kozlov, *Physical Chemistry of the Barrier Discharge* (Verlag DVS, Düsseldorf, 1997).
[7] A. Fridman, *Plasma Chemistry* (Cambridge University Press, 2008).
[8] V. I. Gibalov and G. J. Pietsch, J. Phys. D: Appl. Phys. **33**, 2618 (2000).
[9] A. Chirokov, A. Gutsol, and A. Fridman, Pure Appl. Chem. **77**, 487 (2005).
[10] W. Siemens and Poggendorff, Ann. Phys. Chem. **102**, 66 (1857).
[11] H. E. Wagner, R. Brandenburg, K. V. Kozlov, A. Sonnenfeld, P. Michel, and J. F. Behnke, Vacuum **71**, 417 (2003).
[12] G. Borcia, C. A. Anderson, and N. M. D. Brown, Plasma Sources Sci. Technol. **12**, 335 (2003).
[13] R. Hackam and H. Akiyama, IEEE Trans. Dielectr. Electr. Insul. **7**, 654 (2000).
[14] M. Moreau, N. Orange, and M. G. J. Feuilloley, Biotechnol. Adv. **26**, 610 (2008).
[15] M. Laroussi, M. Kushner, M. Kong, L. Greene, G. Sham, B. Ahlfeld, G. Isbary, W. Stolz, A. Fridma, G. Morfill, K. Stalder, J. Woloszko, S. Kalghatgi, G. McCombs, and M. Darby, *Plasma Medicine: Applications of Low-Temperature Gas Plasmas in Medicine and Biology* (Cambridge University Press, 2012).
[16] E. Moreau, J. Phys. D: Appl. Phys. **40**, 605 (2007).
[17] T. C. Corke, C. L. Enloe, and S. P. Wilkinson, Annu. Rev. Fluid Mech. **42**, 505 (2010).
[18] B. Eliasson and U. Kogelschatz, Appl. Phys. B **46**, 299 (1988).
[19] J. P. Boeuf, C. Punset, A. Hirech, and H. Doyeux, J. Phys. IV **7**, 3 (1997).
[20] N. Na, M. Zhao, S. Zhang, C. Yang, and X. Zhang, J. Am. Soc. Mass Spectrom. **18**, 1859 (2007).
[21] F. Kogelheide, B. Offerhaus, N. Bibinov, P. Krajinski, L. Schücke, J. Schulze, K. Stapelmann, and P. Awakowicz, Plasma Process. Polym. **17**, 1 (2020).
[22] N. Benard, P. Audier, E. Moreau, K. Takashima, and A. Mizuno, J. Electrostat. **88**, 15 (2017).
[23] M. Černák, L. Černáková, I. Hudec, D. Kováčik, and A. Zahoranová, Eur. Phys. J. Appl. Phys. **47**, 22806 (2009).
[24] M. Černák, D. Kováčik, J. Ráhel, P. Sťahel, A. Zahoranová, J. Kubincová, A. Tóth, and L. Černková, Plasma Phys. Controlled Fusion **53**, 124031 (2011).
[25] T. Homola, J. Matoušek, V. Medvecká, A. Zahoranová, M. Kormunda, D. Kováčik, and M. Černák, Appl. Surf. Sci. **258**, 7135 (2012).
[26] N. Benard, A. Mizuno, and E. Moreau, Appl. Phys. Lett. **107**, 233508 (2015).
[27] G. Nayak, Y. Du, R. Brandenburg, and P. J. Bruggeman, Plasma Sources Sci. Technol. **26**, 035001 (2017).
[28] O. Sakai, Y. Kishimoto, and K. Tachibana, J. Phys. D: Appl. Phys. **38**, 431 (2005).
[29] K. Tachibana, T. Nakamura, and H. Motomura, Jpn. J. Appl. Phys., Part 2 **55**, 07LB01 (2016).
[30] H. A. Aboubakr, M. Nisar, G. Nayak, K. V. Nagaraja, J. Collins, P. J. Bruggeman, and S. M. Goyal, Foodborne Pathog. Dis. **17**, 157 (2020).
[31] T. Homola, R. Krumpolec, M. Zemánek, J. Kelar, P. Synek, T. Hoder, and M. Černák, Plasma Chem. Plasma Process. **37**, 1149 (2017).
[32] A. Elkholy, S. Nijdam, E. van Veldhuizen, N. Dam, J. van Oijen, U. Ebert, and L. P. H. de Goey, Plasma Sources Sci. Technol. **27**, 055014 (2018).
[33] K. Shimizu, T. Ishii, and M. Blajan, IEEE Trans. Ind. Appl. **46**, 1125 (2010).
[34] G. Nayak, J. S. Sousa, and P. J. Bruggeman, J. Phys. D: Appl. Phys. **50**, 105205 (2017).
[35] T. Homola, V. Prukner, P. Hoffer, and M. Šimek, Plasma Sources Sci. Technol. **29**, 095014 (2020).
[36] R. Krumpolec, V. Richter, M. Zemánek, and T. Homola, Surf. Interfaces **16**, 181 (2019).
[37] Z. Kelar Tučeková, L. Vacek, R. Krumpolec, J. Kelar, M. Zemánek, M. Černák, and F. Ružička, Molecules **26**, 910 (2021).
[38] G. G. Gebremical, S. Admassu, T. Berhanu, Z. Tučeková, R. Krumpolec, and M. Černák, Eur. Phys. J. D **73**, 99 (2019).
[39] G. G. Gebremical, S. A. Emire, and T. Berhanu, J. Food Qual. **2019**, 3702649.
[40] G. Nayak, H. A. Aboubakr, S. M. Goyal, and P. J. Bruggeman, Plasma Process. Polym. **15**, 1 (2017).
[41] F. Peeters and T. Butterworth, in *Atmospheric Pressure Plasma—From Diagnostics to Applications*, edited by A. Nikiforov and Z. Chen (IntechOpen, 2018).
[42] S. Jahanbakhsh, V. Brüser, and R. Brandenburg, Plasma Sources Sci. Technol. **29**, 015001 (2020).
[43] Y. Akishev, G. Aponin, A. Balakirev, M. Grushin, V. Karalnik, A. Petryakov, and N. Trushkin, Plasma Sources Sci. Technol. **20**, 024005 (2011).
[44] N. Jidenko, M. Petit, and J. P. Borra, J. Phys. D: Appl. Phys. **39**, 281 (2006).
[45] S. Jahanbakhsh, V. Brüser, and R. Brandenburg, Plasma Sources Sci. Technol. **27**, 115011 (2018).
[46] M. Bogaczyk, S. Nemschokmichal, R. Wild, L. Stollenwerk, R. Brandenburg, J. Meichsner, and H. E. Wagner, Contrib. Plasma Phys. **52**, 847 (2012).
[47] Y. Wang, H. Yan, H. Guo, Y. Xu, Z. Fan, and C. Ren, Phys. Plasmas **27**, 033502 (2020).
[48] J. Čech, J. Hanusová, P. Sťahel, and M. Černák, Open Chem. **13**, 528 (2015).

[49]S. Celestin, K. Allegraud, G. Canes-Boussard, N. Leick, O. Guaitella, and A. Rousseau, IEEE Trans. Plasma Sci. **36**, 1326 (2008).

[50]T. Murata, M. Tatsukawa, Y. Okita, and K. Yasuoka, Ozone Sci. Eng. **17**, 575 (1995).

[51]J. C. Laurentie, J. Jolibois, and E. Moreau, J. Electrostat. **67**, 93 (2009).

[52]W. H. Tay, S. L. Yap, and C. S. Wong, AIP Conf. Proc. **1250**, 532 (2010).

[53]G. Huang, Y. Zhou, T. Wang, I. V. Timoshkin, M. P. Wilson, S. J. MacGregor, and M. J. Given, IEEE Trans. Plasma Sci. **44**, 2111 (2016).

[54]P. Reichen, A. Sonnenfeld, and P. Rudolf Von Rohr, J. Phys. D: Appl. Phys. **43**, 025207 (2010).

[55]M. Petit, N. Jidenko, A. Goldman, M. Goldman, and J. P. Borra, Rev. Sci. Instrum. **73**, 2705 (2002).

[56]O. Guaitella, F. Thevenet, C. Guillard, and A. Rousseau, J. Phys. D: Appl. Phys. **39**, 2964 (2006).

[57]S. Celestin, G. Canes-Boussard, O. Guaitella, A. Bourdon, and A. Rousseau, J. Phys. D: Appl. Phys. **41**, 205214 (2008).

[58]A. A. Abdelaziz, T. Ishijima, T. Seto, N. Osawa, H. Wedaa, and Y. Otani, Plasma Sources Sci. Technol. **25**, 035012 (2016).

[59]H. Höft, M. M. Becker, and M. Kettlitz, Phys. Plasmas **23**, 033504 (2016).

[60]S. Pavon, J. L. Dorier, C. Hollenstein, P. Ott, and P. Leyland, J. Phys. D: Appl. Phys. **40**, 1733 (2007).

[61]Z. Wang, C. Ren, Q. Nie, and D. Wang, Plasma Sci. Technol. **11**, 177 (2009).

[62]F. Rodrigues, J. Pascoa, and M. Trancossi, Exp. Therm. Fluid Sci. **90**, 55 (2018).

[63]B. Gilbart, A. Dickenson, J. L. Walsh, and M. I. Hasan, J. Phys. D: Appl. Phys. **54**, 175202 (2021).

[64]R. Tirumala, N. Benard, E. Moreau, M. Fenot, G. Lalizel, and E. Dorignac, J. Phys. D: Appl. Phys. **47**, 255203 (2014).

[65]X. Bian, X. Meng, L. Wang, J. M. K. MacAlpine, Z. Guan, and J. Hui, IEEE Trans. Dielectr. Electr. Insul. **18**, 613 (2011).

[66]X. Bian, Z. He, J. Zhu, X. Pi, S. Wan, and L. Qi, J. Eng. **2019**, 2869.

[67]H. Ryzko, Proc. Phys. Soc. **85**, 1283 (1965).

[68]A. A. Abdelaziz, T. Ishijima, and T. Seto, Phys. Plasmas **25**, 043512 (2018).

[69]Z. Falkenstein and J. J. Coogan, J. Phys. D: Appl. Phys. **30**, 817 (1997).

[70]X. Zhang, B. J. Lee, H. G. Im, and M. S. Cha, IEEE Trans. Plasma Sci. **44**, 2288 (2016).

[71]M. Wicks and F. O. Thomas, AIAA J. **53**, 2801 (2015).

[72]J. Chen and P. Wang, IEEE Trans. Plasma Sci. **33**, 808 (2005).

[73]M. Pavlik and J. D. Skalny, Rapid Commun. Mass Spectrom. **11**, 1757 (1997).

[74]T. Soban and R. Ohyama, Proc. Sch. Eng. Tokai Univ. **41**, 1 (2016). https://www.u-tokai.ac.jp/uploads/sites/11/2021/03/02-11.pdf.

[75]B. R. Maskell, Technical Report No. 701106, 1970.

[76]J. Pawłat, *Electrical Discharges in Humid Environments: Generators, Effects, Application* (Politechnika Lubelska, 2013).

[77]N. Benard, N. Balcon, and E. Moreau, AIAA Paper No. 2009-488 (Orlando, Florida, 2009).

[78]Z. Falkenstein, J. Appl. Phys. **81**, 5975 (1997).

[79]L. Fouad and S. Elhazek, J. Electrostat. **35**, 21 (1995).

[80]I. G. Koo, J. H. Cho, and W. M. Lee, Plasma Process. Polym. **5**, 161 (2008).

[81]R. Ono, Y. Teramoto, and T. Oda, Plasma Sources Sci. Technol. **19**, 015009 (2010).

[82]Z. Tučeková, Z. Kovaľová, A. Zahoranová, Z. Machala, and M. Černák, Eur. Phys. J. Appl. Phys. **75**, 1 (2016).